⌘ *Author's Choice*

THE JOURNAL OF BIOLOGICAL CHEMISTRY VOL. 285, NO. 7, pp. 4964–4974, February 12, 2010

Myosin Motors Drive Long Range Alignment of Actin Filaments*[S]

Received for publication, July 15, 2009, and in revised form, November 16, 2009 Published, JBC Papers in Press, November 24, 2009, DOI 10.1074/jbc.M109.044792

Tariq Butt[‡], Tabish Mufti[§], Ahmad Humayun[§], Peter B. Rosenthal[¶], Sohaib Khan[§], Shahid Khan[‡1], and Justin E. Molloy[¶2]

From the Departments of [‡]Life Sciences and [§]Computer Science, LUMS School of Science and Engineering, Sector U-DHA, Lahore 54792, Pakistan and the [¶]Division of Physical Biochemistry, MRC National Institute for Medical Research, Mill Hill, London NW7 1AA, United Kingdom

The bulk alignment of actin filament sliding movement, powered by randomly oriented myosin molecules, has been observed and studied using an *in vitro* motility assay. The well established, actin filament gliding assay is a minimal experimental system for studying actomyosin motility. Here, we show that when the assay is performed at densities of actin filaments approaching those found in living cells, filament gliding takes up a preferred orientation. The oriented patterns of movement that we have observed extend over a length scale of 10–100 μm, similar to the size of a mammalian cell. We studied the process of filament alignment and found that it depends critically upon filament length and density. We developed a simple quantitative measure of filament sliding orientation and this enabled us to follow the time course of alignment and the formation and disappearance of oriented domains. Domains of oriented filaments formed spontaneously and were separated by distinct boundaries. The pattern of the domain structures changed on the time scale of several seconds and the collision of neighboring domains led to emergence of new patterns. Our results indicate that actin filament crowding may play an important role in structuring the leading edge of migrating cells. Filament alignment due to near-neighbor mechanical interactions can propagate over a length scale of several microns; much greater than the size of individual filaments and analogous to a log drive. Self-alignment of actin filaments may make an important contribution to cell polarity and provide a mechanism by which cell migration direction responds to chemical cues.

In vitro motility assays (1, 2) provide a defined biochemical system to characterize the mechanochemistry of motor proteins and cytoskeletal polymer dynamics (3). The actin filament gliding assay (2) in particular, enables the movement of individual actin filaments to be observed, by fluorescence video microscopy. Rhodamine-phalloidin-labeled filaments are visualized as they move on a microscope coverslip surface that has been coated with randomly oriented myosin molecules. In the absence of Mg-ATP the filaments bind tightly to the surface, but when Mg-ATP is added, the filaments start sliding over the surface. Sequential video images, captured by computer, allow filament positions to be tracked in time using image analysis software so that the speed and direction of filament sliding can be determined. Under standard conditions the movement of an individual filament shows directed motion over a length scale of about 5–10 μm but after the filament has traveled though a contour distance of 100 μm its direction is completely randomized. So within a typical field of view a number of filaments will be seen traveling in a variety of directions. However, by using microfabrication techniques the microscope coverslip surface can be patterned so that filament sliding becomes confined to narrow, linear tracks (4). In living cells, myosins power motile processes in a crowded environment far removed from the conditions that are often used in *in vitro* assays. In particular, within the highly ordered sarcomeres of skeletal muscle cells, actin and myosin filaments are precisely oriented along the length of the cell. This means that external forces generated by muscle act along the axis of its fibers. Muscle cells are highly specialized to produce large external forces but every cell in the body contains myosin and actin and of the 39 human myosin genes most of them encode for so-called non-muscle myosins. Myosins are involved in a wide variety of cell motilities including vesicle trafficking and cell migration. The molecular mechanism of force generation by actomyosin has been extensively studied and the current view is as follows. Myosin binds actin ATP hydrolysis products (ADP and P_i) bound at its catalytic site; as the products are released the light chain binding region of the molecule swings through an angle of about 60° in a process known as the "power stroke"; the power stroke generates a relative sliding motion between the tail of the myosin and its attachment point with actin between 5 and 30 nm and a force of around 2 to 5 piconewtons; once the power stroke is complete a fresh ATP molecule binds to myosin, which causes it to detach from actin and reset its conformation (known as the "recovery stroke"); it can then undergo further cycles of interaction with actin as above. The time myosin spends tightly bound to actin compared with the total ATPase cycle time is called the "duty cycle ratio." Fast acting myosins like those found in muscle typically have a low duty cycle ratio, whereas processive motors like myosin V have a high duty ratio (5). The myosins known to

* The work was supported by a Higher Education Commission-British Council Link grant in "Bionanotechnology" (to Sh. K.), Lahore University of Management Sciences, School of Science and Engineering, Computer Science Department for research assistant stipends (to A. H. and T. M.), and a Medical Research Council, UK, grant-in-aid (to J. E. M. and P. B. R.).

⌘ *Author's Choice*—Final version full access.

[S] The on-line version of this article (available at http://www.jbc.org) contains supplemental movies.

[1] To whom correspondence may be addressed. E-mail: shahidkh@lums.edu.pk.

[2] To whom correspondence may be addressed: MRC NIMR, The Ridgeway, Mill Hill, London NW7 1AA, United Kingdom. E-mail: jmolloy@nimr.mrc.ac.uk.

be involved in cell migration (myosin I, IIa, IIb, and IIc) (6) contribute to extension or retraction of the lamellipodium by driving the relative flow of cortical actin filaments past the plasma membrane and cell-substrate adhesions (7). The myosin II proteins localize by immunofluorescence in a punctate pattern at cell edges and their cellular role is under active study (8). Several other unconventional myosins such as myosin V, VI, VII, IX, and X may also play critical roles in formation and maintenance of the lamellipodial structure (9). The cortical actin forms a dense meshwork at the leading edge of the cell and the local actin concentration reaches 100 μM. This meshwork is stabilized and remodeled by various actin-related and actin-binding proteins (10). Actin polymerization-depolymerization and actin bulk flow have been proposed to drive lamellipodial movements, in addition to or instead of myosin (11–13). Finally, accessory protein complexes involved in intracellular signaling couple actin dynamics to physiological function (14–17) and either activate or inhibit actin filament turnover and/or actomyosin interactions.

Concentrated F-actin solutions undergo gel-sol phase transitions (18) and the rheology and viscoelastic behavior (19) has been well studied. It is known that actin filaments become aligned by flow and the shear modulus is strongly dependent on filament length (20). It is of interest whether filament alignment might arise spontaneously within the cell cortex due to shear forces and filament movement generated by actomyosin interactions. We have addressed this issue using an *in vitro* actin filament gliding assay in which actin filament density approaches that found in the cell cortex. We used computerized analysis of filament motility under a variety of experimental conditions in which filament movement is actively driven by surface-attached skeletal muscle, myosin II molecules.

A number of algorithms have been described to track actin filament movement in *in vitro* motility assays (21–24) and only a limited number of these methods have the capability to simultaneously measure the motion of many particles captured on video. This ability is essential for the present study, as we wish to investigate cooperative movements of many filaments simultaneously. We developed measures of the orientation of motile filament tracks at the single and population level. We used an established centroiding method (25) and found this worked well for short filaments that could be treated as rigid rods, but worked less well for long, highly curved, filaments. So, we developed a new algorithm that works from skeletonized filament outlines and this approach enabled us to quantify filament velocity and direction at high filament densities. Our results give insight into how cortical F-actin might be organized to produce the required, concerted, force found in lamellipodial extensions of translocating cells.

MATERIALS AND METHODS

Experimental Solutions and Protein Preparation—All chemicals were from Sigma unless otherwise noted. Our motility assays were conducted using established assay buffers and conditions briefly: 10× AB^- (a 10× concentrated stock solution) was composed of 250 mM imidazole-HCl, 250 mM KCl, 10 mM EGTA, 40 mM $MgCl_2$, pH 7.4. 10× AB^+ was the same as AB^- but with 20 mM Mg·ATP added. These stock solutions were stored as 1-ml aliquots at −20 °C. Both stocks were treated identically, so termed generically as AB, as follows. On the day of the experiment, 1 ml of 10× AB stock was thawed and mixed with 9 ml of deionized water and degassed for 5 min. The solutions were then immediately transferred to 10-ml hypodermic syringes fitted with narrow-bore needles to reduce contamination with atmospheric oxygen. To reduce photobleaching during the fluorescence imaging experiments (see below) an oxygen scavenger system was added to 1-ml aliquots of the degassed AB. This required addition of the following chemicals to a final concentration of 20 mM DTT, 0.2 mg/ml of glucose oxidase, 0.5 mg/ml of catalase, 3 mg/ml of glucose, 0.5 mg/ml of bovine serum albumin. The oxygen scavenger containing solutions, termed AB/GOC, were then stored in 1-ml hypodermic syringes fitted with narrow-bore needles to reduce oxygen contamination. The syringes were warmed to ~30 °C for 5 min by rolling between the hands so that the enzymatic removal of dissolved oxygen proceeded rapidly. All syringes were stored on ice and during the course of the experimental day, oxygen scavenger containing solutions were replenished, as needed, using the degassed AB contained in the 10-ml syringes.

Actin, myosin, and the proteolytic subfragment of myosin called heavy meromyosin (HMM)[3] were prepared from rabbit back and leg fast skeletal muscles by established protocols (26, 27). Synthetic myosin thick filaments were created by gradual dilution of the myosin stock (5 mg/ml) made up in a high salt buffer (AB^- supplemented with 1 M KCl) to a final concentration of 100 mM KCl (0.5 mg/ml of myosin). The myosin formed regular, dispersed, synthetic thick filaments that were visualized using negative stain, electron microscopy. Monomeric, globular actin (G-actin) stock (4.5 mg/ml to ~100 μM, stored as 50-μl aliquots by rapid freezing at −80 °C) was polymerized to form filamentous actin (F-actin) by the addition of 1/10th volume (*e.g.* 5.5 μl) of 10× AB^+. Subaliquots of the F-actin stock were then stabilized by addition of equimolar (to G-actin, monomer) amounts of either rhodamine-phalloidin or unmodified phalloidin. The rhodamine-phalloidin-labeled F-actin aliquot was wrapped in aluminum foil to reduce photobleaching by ambient light. The HMM stock (4 mg/ml, stored as 50-μl aliquots by rapid freezing at −80 °C) was thawed on the day of the experiment. All solutions were kept on ice during the experiment, but warmed to room temperature before addition to the experimental flow cell (see below).

Experimental Flow Cell Construction—Disposable microscope flow cells were constructed using a pre-cleaned microscope slide (25 × 75 mm; "Superfrost," Menzel-Glaser GmbH and Co., Braunschweig, Germany) and a No. 1 coverslip (22 × 22 mm; Menzel-Glaser). The coverslip was coated with a 1% nitrocellulose solution diluted from a 10% stock in amyl acetate (Ernest F. Fullham Inc., Clifton Park, NY). The nitrocellulose was applied as a 2-μl droplet to the top edge of the coverslip spread over the surface of the coverslip in a single sweep using the pipette tip as a wand. The nitrocellulose-treated coverslip was then fixed to the central region of the slide using two strips of double-sided tape (Permanent Double Sided Tape, number

[3] The abbreviations used are: HMM, heavy meromyosin; AB, assay buffer; GOC, glucose oxidase and catalase oxygen scavenger solution.

34-8507-7367-3, Scotch 3M, Bracknell, Berkshire, UK) so that a channel (10 mm × 22 mm × 100 μm deep, *i.e.* 22 μl volume) parallel to the long axis of the microscope slide was formed between the slide and coverslip with the nitrocellulose surface innermost. An upright fluorescence microscope (Axioskop 40, Carl Zeiss Ltd., Welwyn Garden City, Herts, UK) arrangement used in these experiments requires that the coverslip forms the upper surface of the flow cell (*i.e.* adjacent to the microscope objective lens), whereas the slide is on the lower surface fixed firmly to the microscope stage. Experimental solutions were exchanged using a pipette to apply solution at one end and filter paper to remove solution from the other.

Microscopy—Assays were performed using an Axioskop 40, fluorescence microscope with a PlanNeofluar 100 × 1.3 numerical aperture objective fitted with a custom laser excitation system consisting of a frequency doubled neodymium:yttrium aluminum garnet laser (λ = 532 nm, 20 milliwatts, continuous wave transverse emission mode 0,0, Suwtec, SP3Plus, Tunbridge Wells, Kent, UK) that entered the fluorescence light path using a custom-built adaptor. Fluorescence emitted from the rhodamine-phalloidin-labeled actin filament specimen was collected through the same objective lens and passed through a dichroic and bandpass filter (560DRLP and 595AF60, Omega Optical, Brattleboro, VT) to be imaged onto a charge coupled device camera (Watec WAT 902H Ultimate, Alrad Instruments, Newbury, Berks, UK). Sequences of video frames were captured using a frame grabber card (Picolo, Euresys, Multipix Imaging Ltd., Petersfield, Hampshire, UK) and recorded onto a computer hard disc. The laboratory was air conditioned and the experimental temperature kept at 23 °C. Synthetic myosin filaments were deposited on carbon-formvar-coated 400-mesh grids, negatively stained with 1% uranyl acetate and visualized at ×30,000 magnification at 120 kV in an FEI Spirit™ transmission electron microscope.

In Vitro Motility Assay Standard Conditions—HMM was bound to the nitrocellulose-coated coverslip by flowing 25 μl of 200 μg/ml of HMM in AB^- into the flow cell and incubating for 1 min. For experiments using synthetic myosin thick filaments, 0.5 mg/ml of myosin filaments was added to the flow cell and incubated for 1 min followed by elution with one flow cell volume of AB^-. The flow cell surfaces were then "blocked" by flowing 2 washes of 25 μl of 1 mg/ml of bovine serum albumin in AB^- into the flow cell and leaving for 2 min. Finally 25 μl of AB^-/GOC solution was added containing rhodamine-phalloidin-stabilized actin filaments (20 nM G-actin concentration). In the absence of ATP the actin filaments bound tightly to the coverslip surface and could be viewed by fluorescence microscopy. Finally, an AB^+/GOC solution containing various levels of F-actin stabilized with phalloidin was added to the flow cell. The Mg-ATP-containing, AB^+, solution initiated actin filament sliding and the nature of the sliding motion could be recorded using fluorescence video microscopy. Actin samples were treated identically to ensure that the rhodamine-labeled fraction reported the properties of the bulk by acting as a minority labeled species. This procedure was adopted because at high concentrations of labeled filaments high background fluorescence meant that individual filaments could no longer be identified and tracked.

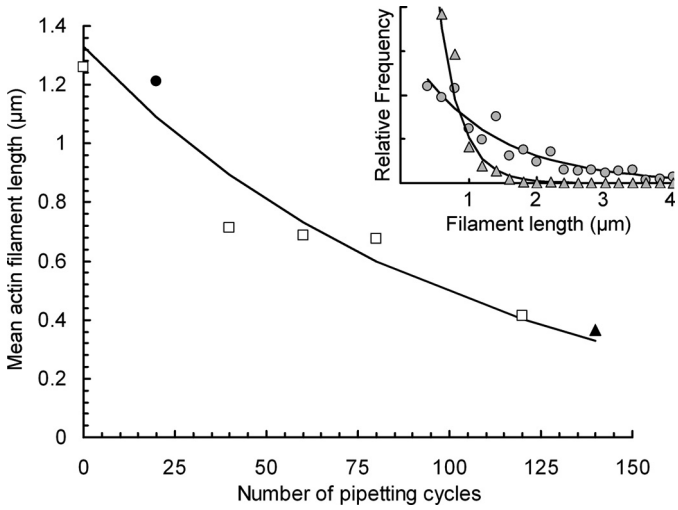

FIGURE 1. Decrease in the mean actin filament length due to mechanical shearing caused by repeated pipetting is plotted as a function of the number of pipetting cycles (*square symbols*, except the *circle* and *triangle* at 20 and 140 cycles, which are highlighted to refer to the corresponding histograms of length distributions shown in the *inset*). *Inset* shows the distribution of filament lengths for 20 (*circles*) and 140 (*triangles*) pipetting cycles (corresponding to the two highlighted data points in the main figure). The length distributions for all treatments were approximately monoexponential (shown in these example plots by the *solid fitted lines*).

In some experiments, actin filament length was altered by mechanically shearing the filaments by repeated manual pipetting. The resulting filament length distribution was quantified by analyzing video images of F-actin bound to the motility assay surface in AB^-/GOC (see above). The filament length distribution was approximately exponential implying a constant probability of breakage per unit length. We found that by using a standard 1-mm tip diameter 200-μl Eppendorf pipette and varying the number of pipetting cycles from 20 to 140 the average filament length could be shortened in a nonlinear but controllable fashion from about 3 μm down to 0.5 μm. By plotting mean filament length against the number of pipetting cycles we could derive an empirical relationship that enabled us to generate filaments of known average filament length (Fig. 1). The shear modulus is strongly dependent on length. It has been reported to vary by a factor of 100 over the 0.5 to 4-μm length range (20).

Filament populations employed in our experiments fell in this length range. Filament lengths were measured from skeletonized outlines using scripts written in ImageJ and Matlab. Length distributions were subsequently analyzed in Excel™ employing the non-linear, least squares fitting procedure, "Solver."

RESULTS

Quantitative Measurement of Actin Filament Orientation—GMimPro software (25) was used to track rhodamine-phalloidin-labeled F-actin filaments of different lengths. In addition to mechanical shearing, the filaments were further shortened in the flow cell due to surface interactions with HMM molecules. Actin filaments, <2 μm long, approximated rigid rods because this is well below the persistence length of actin (~17 μm (28)).[4]

[4] Persistence length is the distance over which the curvature of a filament due to thermal motion becomes clearly visible and one end of the filament points in a random direction compared with the other end.

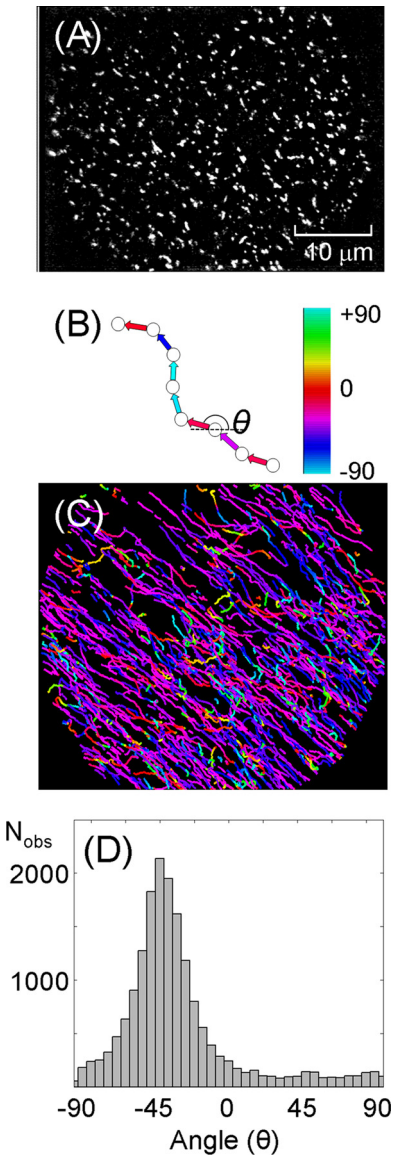

FIGURE 2. *A*, a single video frame (40-ms exposure) shows the appearance of individual, fluorescent actin filaments, which move during successive video frames (see supplemental movies). *B*, individual filaments were automatically tracked by computer and filament positions on successive frames (shown as *circles*) were linked to estimate the movement vector. The color key shows how angular values from −90° to +90° were encoded. *C*, the angular vector between pairs of consecutive centroid locations were color-coded (as in *B*) and plotted as a continuous track to highlight the path of each filament. The tracks shown are from a 100-frame video sequence recorded at 25 frames/s. *D*, histogram showing the distribution of angles, θ, for the tracks shown in *C*.

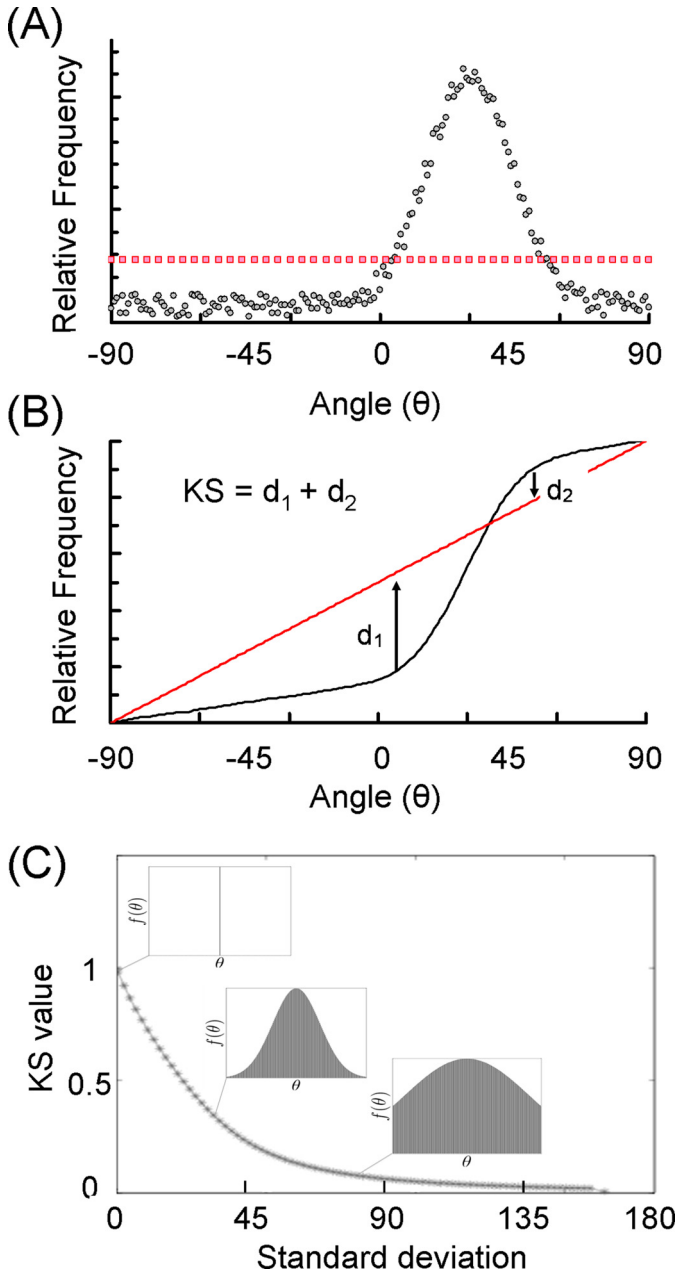

FIGURE 3. *A*, probability distributions of angle, θ, were modeled to simulate filament sliding data (similar to the data shown in Fig. 2*D*, shown here as *gray circles*) and compared with a model in which each angle is equally likely (*i.e.* the filament movement is completely random, shown as *red squares*). *B*, cumulative distributions derived by summation of the probability distributions shown in *A*. The Kuiper statistic (KS) = $d_1 + d_2$ provides a measure of the deviation of a measured distribution (*black line*) from the idealized, random distribution (*red line*). *C*, a representation of the KS values evaluated from modeled distributions with increasing variance (s^2) ranging from a δ function (s = 0, KS = 1), and progressively oriented Gaussian distributions (s = 30°, KS = 0.34; s = 80°, KS = 0.08).

Individual filament paths could be readily obtained by GMimPro. Once the centroid of each filament was located in each frame, locations were linked frame-by-frame to construct filament paths in time. Then the immediate velocity of each filament as it moved along its path was calculated together with its immediate angle of motion with respect to the horizontal (*e.g.* the pixel row or video line) (Fig. 2, *A*–*D*). This information was accumulated for each filament in the entire video sequence so that the orientation distribution could be established for the entire population of filaments that had been tracked in a given video sequence (Fig. 2).

To determine the degree of "orientedness" exhibited by a population of F-actin filaments in a video sequence, we compared the orientation distribution with an idealized uniform distribution. A uniform distribution for the angle of motion would imply that there was no preferred orientation of filament movement, *i.e.* the filaments were moving in random directions. If the distribution varied significantly from the uniform pattern, it would indicate that there was a preferred orientation of motion (Fig. 3*A*). We used Kuiper's test (29) to compare the observed distributions of movement directions with a uniform

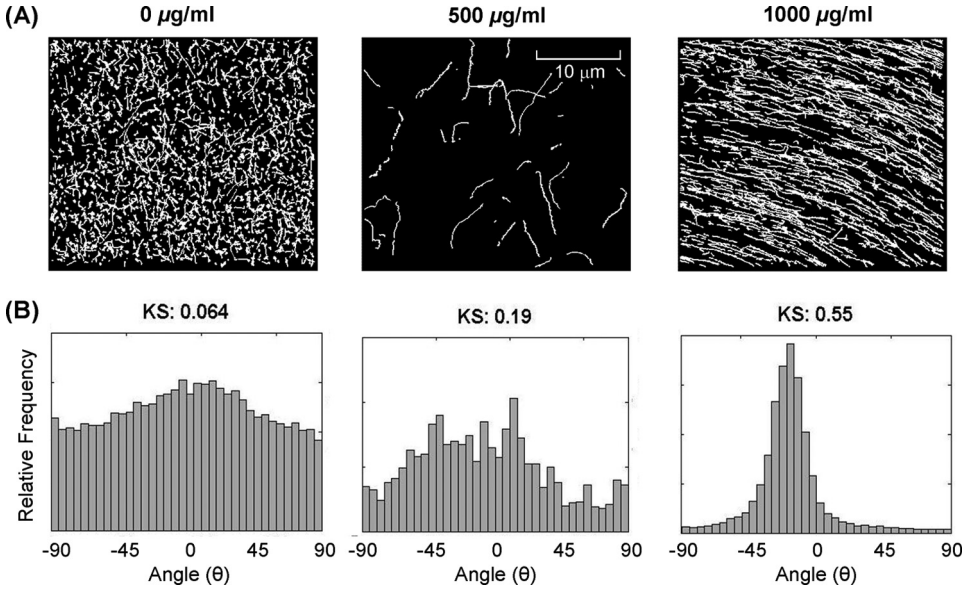

FIGURE 4. *A*, actin filament tracks at different concentrations of added plain F-actin. The *left-hand panel* shows filament tracks obtained by visualizing and automatically tracking rhodamine-phalloidin-labeled actin filaments under standard *in vitro* motility assay conditions, when there was no added plain F-actin in the bulk solution (designated 0 μg/ml); the filament sliding velocity was 1.9 $\pm$ 0.01 μm/s. The *center panel* shows tracks recorded in the presence of 500 μg/ml of added plain F-actin (velocity = 2.62 $\pm$ 0.04 μm/s). The *right-hand panel* was with 1000 μg/ml plain F-actin (velocity = 2.83 $\pm$ 0.01 μm/s). The *tracks* appear shorter in the record at 0 μg/ml (added F-actin) due to track fragmentation, which occurs when motile filaments moved over stuck ones. The apparent variation in the number of tracks obtained in the different experiments where plain F-actin was added is due to exchange of the labeled and plain F-actin between the surface and the medium. *B*, the graphs show the distribution of track angles, θ, summed over the population (corresponding to the panels above), and the associated Kuiper statistic (*KS*) values.

distribution. Kuiper's (29) test is a modified version of the Kolmogorov-Smirnov test, but with the advantage that it is cyclically invariant. Thus, rotation of the data, for example, produced by rotating the slide or selecting a different reference axis, does not change the Kuiper statistic value.

To compute the statistic for the Kuiper test, we first determined the cumulative distribution functions, both for the orientation distribution and the uniform distribution. The maximum deviation between the two cumulative distribution functions is measured in both directions, shown by d_1 and d_2 (Fig. 3*B*). The key difference in comparison to the Kolmogorov-Smirnov test is that the Kuiper test uses the sum of d_1 and d_2 as the test statistic. This ensures that under cyclic transformation (*i.e.* a circular shifting of the angular axis), the test statistic will remain exactly the same. To verify the suitability of the Kuiper test as a measure of the group alignment of the filaments, we generated modeled orientation distributions by progressively increasing the variance of a Gaussian function, truncated to the finite range of our axis. This resulted in a set of histograms starting from an ideal δ function and getting wider and closer to a uniform distribution. A few histograms from this set are shown in the *insets* in Fig. 3*C*. The Kuiper value decreased from unity as the variance of the Gaussian distribution increased from a δ function (Fig. 3*C*). For a perfectly uniform distribution, the Kuiper value was zero, as expected.

Orientation Dependence as a Function of Filament Surface Density—To investigate the effect of increasing the surface density of actin filaments on motility we used a constant amount of rhodamine-phalloidin F-actin (0.06 μg/ml, termed "labeled filaments") mixed with varying amounts of phalloidin-stabilized F-actin (from 0 to 1 mg/ml termed "plain F-actin"). Under standard *in vitro* motility assay conditions (*i.e.* with no additional plain actin) the labeled filaments moved randomly over the surface (Fig. 4). Our initial observation was that when plain F-actin was added to the flow cell the labeled filaments started to move in an oriented fashion (Fig. 4, *A* and *B*). The Kuiper statistic increased dramatically, indicating that the filament population had started to move in a preferred direction, and at the highest concentrations of plain F-actin used the degree of filament alignment became obvious even by casual visual inspection (Fig. 4).

At 500 μg/ml of added plain F-actin the labeled filaments began to move more rapidly and in a more persistent fashion across the field of view (Fig. 4, *center panels*). The variation in angular direction measured for individual filaments, as they moved across a field of view, was histogrammed to indicate the degree of individual persistence of motion direction (Fig. 5, *A* and *B*). As described earlier, at high concentrations of added plain F-actin (1 mg/ml) all of the filaments within a field of view moved in a highly oriented fashion (*e.g.* Fig. 4, *right-hand panels*). Under these conditions all filaments within the field of view tended to travel along the same vector. Even so, the orientation effect seemed evident even at lower concentrations.

We quantified the concentration dependence of the alignment phenomenon by varying the concentration of plain F-actin added to the bulk solution. The Kuiper statistical test was then used to provide a quantitative readout of orientedness.

The motility assay was started under standard assay conditions (*i.e.* no added plain F-actin) and a reference measurement of motility made. Then AB^+/GOC buffer containing different amounts of plain F-actin was added to the flow cell and the movement of labeled filaments in different fields of view measured at different times after addition was recorded so that spatial and temporal effects could be monitored. At low concentrations (500 μg/ml) of added plain F-actin a small but significant effect on filament alignment was noted (as in Fig. 4). As the concentration of plain F-actin was increased further, the Kuiper statistic rose sharply to a saturation value (~1 mg/ml added plain F-actin) (Fig. 6). The amount of plain F-actin that binds at the coverslip surface depends upon its binding affinity and bulk concentration. So, the relationship between the Kuiper statistic value and the amount of surface-bound F-actin is empirical. The important finding is that self-alignment of filament sliding becomes very marked at concentrations typical of those found *in vivo* (0.1 to 1 mg/ml = 2.5 to 25 μM actin).

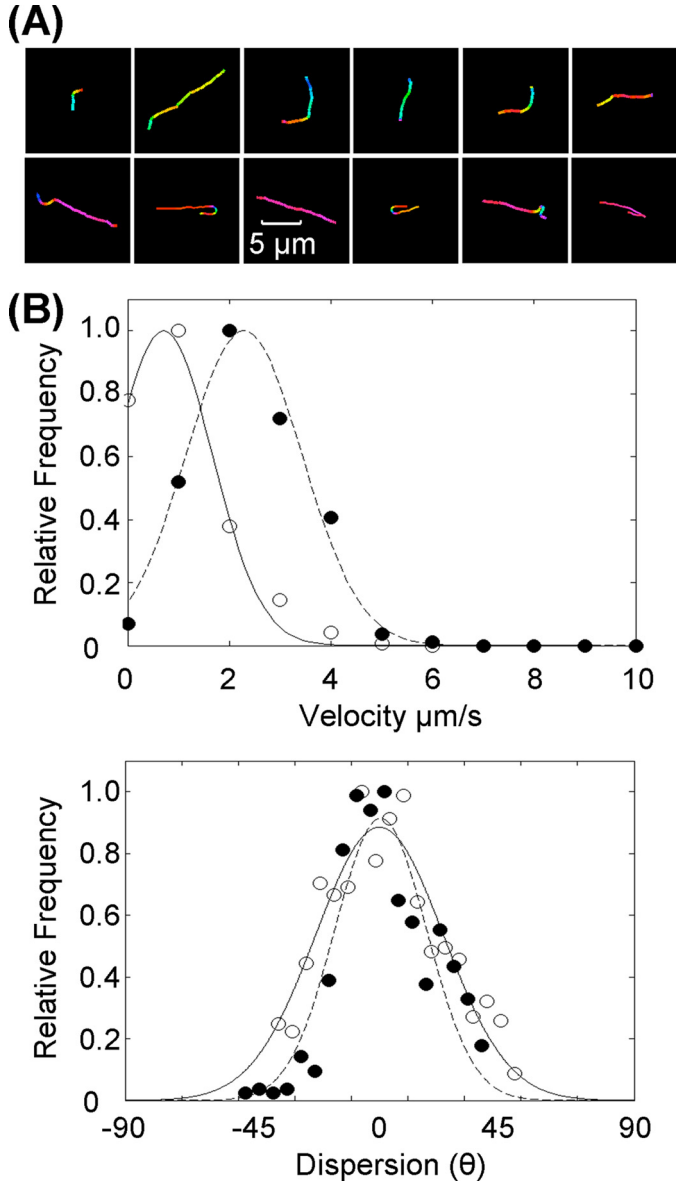

FIGURE 5. *A*, single actin filament tracks obtained under conditions with no additional plain F-actin (*upper*) and 1000 μg/ml of plain F-actin (*lower*). In the absence of added plain F-actin the filament tracks meander; whereas in the presence of plain F-actin the paths are straighter, but undergo either brief lateral excursions, or abrupt reversals of direction. *Colors* denote angular values of θ described in Fig. 2*B*. *B*, histograms of sliding velocities (*upper graph*) indicate the presence of plain F-actin significantly increases speed (12 filaments, ~1000 data points, for each condition). Histograms of angular dispersion derived from the same data set indicate the persistence in sliding direction for individual filaments (*lower graph*). Values in both cases were estimated using a three-point sliding average through successive position centroids. The *lines* are least squares, best fits, to Gaussian distributions:0 μg/ml (*open circles*, *solid line*) and 1000 μg/ml (*closed circles*, *dotted line*). A χ-squared goodness of fit to the Gaussian fit for the data from the sample without plain F-actin is 3 ($p = 0.995$), whereas that for the other sample to the same fit is 16 ($p = 0.5$).

We suspected that part of the variance in our data might be attributable to variation in plain F-actin and labeled filament length. The degree of alignment (Kuiper statistic) correlated with the average length of the labeled filaments under a given set of conditions. Actin filaments become shorter during the course of the motility assay because they are sheared by the forces exerted by the myosin motors. In fact, long filaments are often seen to break as they move during the assay. We typically observed a roughly 33% decrease in filament length after 10 min in the experimental flow cell and we assume that phalloidin-stabilized and rhodamine-phalloidin-stabilized filaments behaved similarly.

To explore the effect of filament length on the degree of filament alignment we worked at saturating concentrations of added plain F-actin (1 mg/ml) and varied the filament length in both labeled and plain F-actin stocks, systematically, by shearing the actin filaments using the pipetting method described earlier (see Fig. 1). We found that the degree of alignment of the motility was greatly reduced at shorter filament lengths. The Kuiper statistic fell from 0.46 (at 1.3-μm mean filament length) to 0.05 (at 0.5-μm mean filament length), *i.e.* from highly aligned motion to virtually random motion (Fig. 6).

Pattern of Single Filament Sliding at Low and High Filament Surface Densities—As described above, under standard *in vitro* motility assay conditions (*i.e.* with no added plain F-actin), labeled filaments moved randomly over the surface. However, when plain F-actin was added, filament sliding speed was smoother and excursions from the preferred direction of travel were less common. At high concentrations of added plain F-actin, filament motion became highly oriented and filaments would occasionally reverse their direction of travel by rapidly turning through 180° (head-over-tail). Centroid-based tracking (using GMimPro) was satisfactory for populations of short filaments (<1 μm mean length) seeded at low surface density in the motility assay. However, longer filaments at higher surface density (*i.e.* more filaments per field of view) resulted in errors in displacement and orientation determination due to filament curvature and failure of the tracking procedure due to crossover events (*e.g.* as one filament passed over another). The persistence length of F-actin in aqueous solution is ~17 μm (28), but significant filament curvature was observed in the motility assay for surface-bound filaments longer than 3 μm due to forces generated by the myosin molecules during filament gliding. To track highly curved filaments we developed an algorithm that took into account the filament shape and crossing events. In brief, this algorithm segments the filaments from the background using a thresholding method, and then applies a region-based correspondence algorithm to track them frame-to-frame. The key difference between centroid-based correspondence and our algorithm is the use of region correspondence; at each subsequent frame, the entire region information is used to determine the boundary of a filament, rather than just the centroid. This allows the assignment of multiple object identities to a single connected shape that results when images of two filaments merge (called occlusion). For such cases, we were able to use the shape statistics before the occlusion to resolve individual objects after multiple objects produced a single, merged pattern. The end result is a reliable determination of the positions of the filaments, even under conditions of occlusion (Fig. 7). The two algorithms were used interchangeably depending on population characteristics. Full details of the tracking algorithm used here will be described fully elsewhere.[5]

[5] A. Humayun, Sh. Khan, J. E. Molloy, and So. Khan, unpublished data.

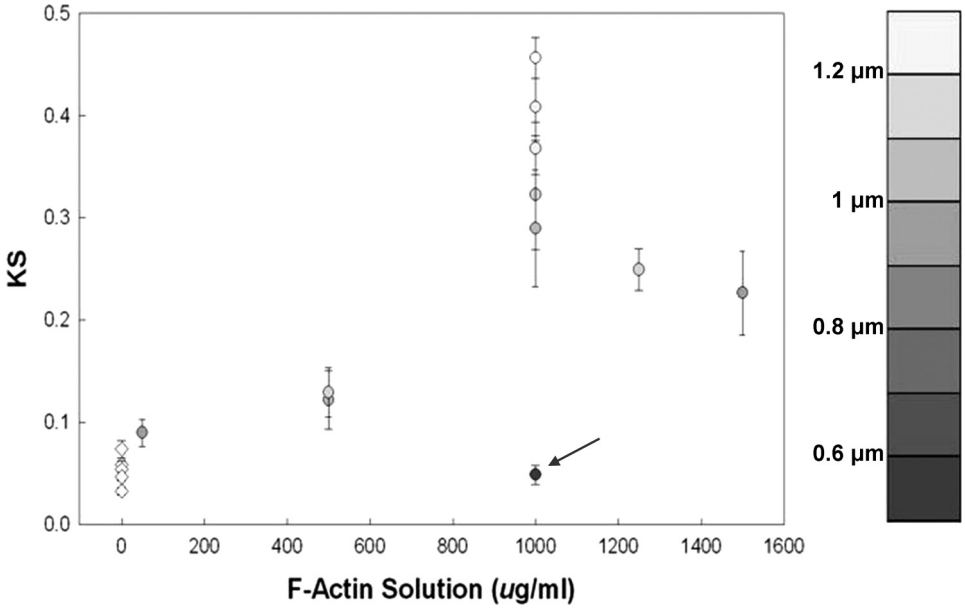

FIGURE 6. **Dependence of the Kuiper statistic (*KS*) on concentration of added plain F-actin and mean actin filament length (*gray scale, right panel*).** Orientedness of filament sliding, indicated by the KS value, depends upon both the amount of unlabeled F-actin and filament length. Scatter in the data at a given concentration of added F-actin can be explained by variation in actin length due to filament shearing during the motility assay. A 2-fold decrease in length from the normal starting value of 1.3 to 0.7 μm (at 1000 μg/ml of plain F-actin) was achieved by shearing the filaments by repeated pipetting (see Fig. 1). This resulted in almost complete loss of oriented sliding behavior (*arrow*).

Temporal Properties of Oriented Filament Sliding—Increasing the amount of plain F-actin added to the flow cell increases both the bulk concentration and the surface density of actin. Because myosin driven motility only occurs at the coverslip surface we investigated the influence of plain F-actin in the bulk compared with the surface-bound fraction. We flowed in plain F-actin solution in the absence of Mg-ATP (AB^-/GOC); allowing time for surface attachment via the myosin heads. Then the solution was washed out and replaced by a solution containing the rhodamine-labeled filaments. Again, these were given sufficient time to bind to the remaining, available, myosin molecules. Sliding motility was then initiated by flow-through Mg-ATP buffer (AB^+/GOC). Filament movement was then recorded from different locations within the flow cell. Initially, randomly oriented sliding motility was observed. But, filament sliding then became progressively orientated over a subsequent period of several minutes. At longer times, motility was highly oriented regardless of position within the flow cell. The angle of preferred orientation varied from one position to the next as different regions of the coverslip surface were inspected (Fig. 8).

This showed that the filaments orient themselves in the absence of plain F-actin in bulk solution; a high surface density of F-actin alone was sufficient to induce oriented motion. We noted that there was variation in the time required to align a population of filaments at different regions within the flow cell (*e.g.* position 3 aligned slower than position 2; see Fig. 8*B*) presumably due to heterogeneity in the surface density of F-actin or myosin coating present on the nitrocellulose substrate. However, as noted above, after a 20-min incubation time, the whole flow cell sample showed aligned patterns of movement. Different regions of the flow cell showed different directions of orientation and by carefully positioning the microscope slide the field of view could be adjusted such that neighboring domains of differently oriented motion could be visualized simultaneously.

Temporal Stability of Aligned Domains Depends upon Their Size—The stability of the ordered domains was examined by a time lapse recording method in which 100 frames of video (4 s) were collected and then the illumination and camera were gated off for a period of 30 s and the process repeated so that the same region could be viewed for extended periods of time without photobleaching. We observed that the orientedness remained relatively constant but the preferred angular direction (mode) changed dramatically. The orientation swung through large angles on the time scale of minutes (Fig. 9).

Of most interest were regions where neighboring domains with radically different preferred angles of motion interfaced (Fig. 10). In such regions we could observe the effect of collisions between neighboring domains. Fig. 10 shows an example where two adjacent domains interact (Fig. 10*A*) and how after a period of 6 s one of the domains dominates the overall pattern and filaments became reoriented to the preferred angle of that one domain.

To test if the alignment phenomenon observed using HMM also occurs in the presence of myosin filaments we performed assays using flow surfaces coated with synthetic thick filaments. These conditions are closer to the physiological state of myosin IIa and IIb in living cells in which myosin forms discrete mini-filaments. We found that strong alignment of actin motility again occurred when >1 mg/ml of unlabeled actin was present (Fig. 11).

DISCUSSION

Our conclusions rely upon use of quantitative measures of actin filament sliding within an *in vitro* motility assay system. Following our initial observation that filament sliding becomes strongly oriented when high surface densities of plain F-actin are present in this assay system, we defined a measure of orientedness based on the Kuiper statistic. This analytical tool enabled local domains of oriented motion to be identified so that the evolution of oriented patterns of movement could be followed in space and time. The fascinating aspect of the self-orienting system is that the length scale over which the patterns emerge are similar to the size of the leading lamella of a migrating mammalian cell. We found that oriented patterns of F-actin movement evolve with time and that the collision of differently oriented domains gives rise to new patterns of movement. This observation gives insight into how signals in one region of the leading lamellae might propagate across the cell via mechanical

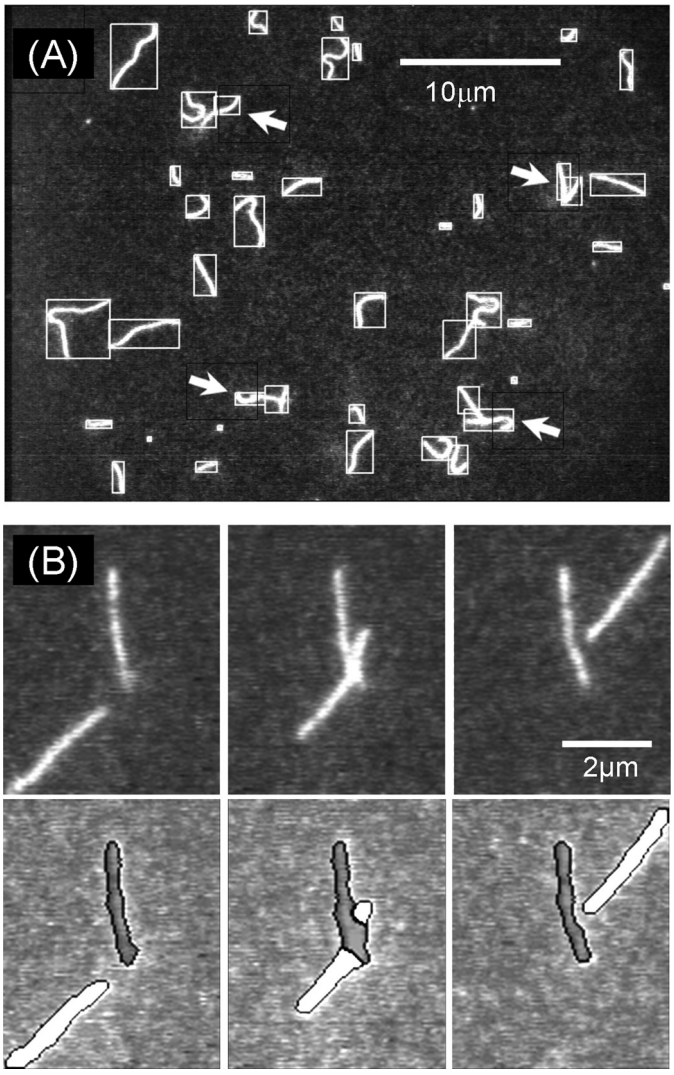

FIGURE 7. *A*, a single video frame showing labeled F-actin filaments and object recognition as discrete objects (*white boxes*). *Arrows* indicate locations in the image where two or more filaments overlap each other. Each filament was resolved separately, as indicated by the superimposed bounding *boxes*. *B*, three video frames show the path of a moving filament as it crosses an immobile filament (*upper panels*). The digitized, segmented images (corresponding *lower panels*) show how the two filaments were recognized as discrete objects. In this case, the sliding filament (*white coding*) was continuously tracked even as it passed over the stuck filament (*dark gray coding*).

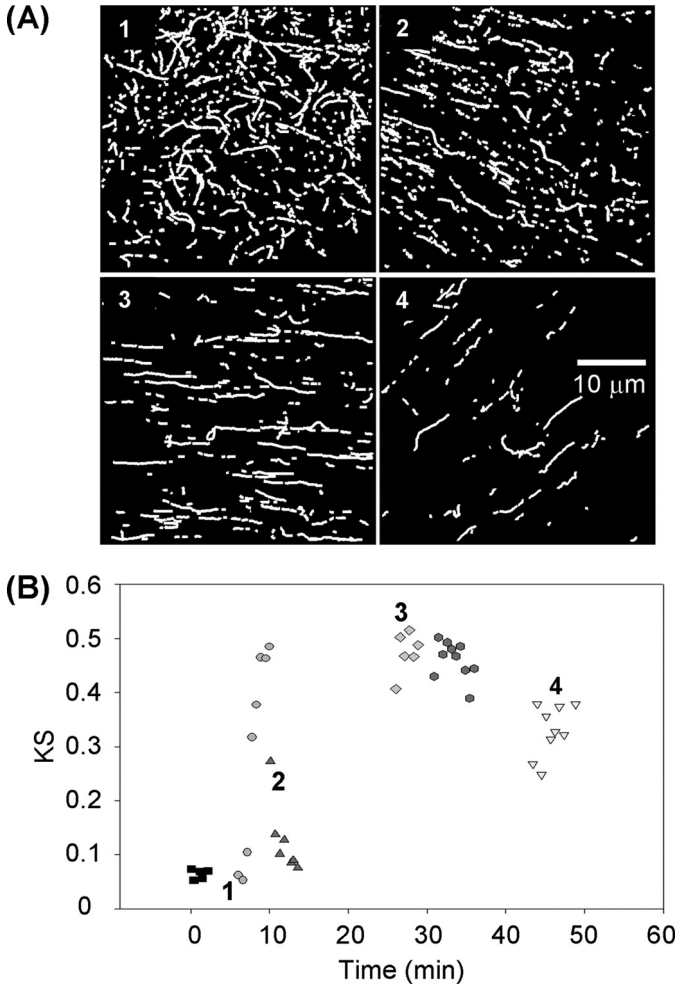

FIGURE 8. *A*, track records from four different positions in a flow cell are shown. The evolution of oriented sliding motility was determined by plotting the Kuiper statistic (*KS*) measured at different regions of the flow cell at different times. *B*, movement was increasingly well ordered (higher KS) at later times, regardless of position within the flow cell and the preferred angle of movement (relative to the microscope axis) varied widely from one field of view to another. The *numbers* on the graph correspond to the images shown in *A*. Clusters of points represented by the same symbol type were generated from separated video sequences (lasting 5 s, recorded at 25 frames/s) obtained from the same region (40×40 μm^2 area) of the coverslip with a gap ($\sim$20 s) between each recording sufficient to allow new filaments to enter the field of view. The transition from random (KS $<$ 0.1) to highly oriented (KS $=$ 0.5) movement is abrupt (about 8 min in this example) and occurs at around the same time in different regions of the flow cell. Filament sliding velocity was $\sim$2.5 μm/s in all records; treatment with 1 mg/ml of unlabeled F-actin was used.

interaction between filaments so that cell migration might be steered toward or away from a chemical cue.

At actin concentrations of above 20 μM we found that movement of rhodamine-phalloidin-labeled actin filaments became locally aligned and ordered domains formed in which movement was strongly oriented along one preferred axis. The degree and direction of alignment evolved with time and was clearly driven by the sliding motion generated by actomyosin interactions. A few tens of seconds after the addition of high background concentrations of plain F-actin; myosin driven movement of the filaments at the coverslip surface started to show increased speed and the direction of filament travel began to follow a straighter trajectory path. After a few minutes, movement of filaments within a typical field of view (100×100 μm) became strongly aligned along one preferred direction. The alignment direction was random with respect to microscope axis and once established, was maintained until Mg-ATP was depleted by actomyosin ATPase activity. In any particular experimental sample, discrete domains were observed with different alignment angles relative to each other. Domain alignments fluctuated on the second to minute time scale and variation in preferred angle with time depended upon the domain size. The degree of alignment of the population increased dramatically with actin concentration (and F-actin surface density) and the effect was maximal at concentrations of actin similar to those found in the leading lamella of the living cell (1 mg/ml $=$ 25 μM actin).

The behaviors reported here are in contrast to the sharp gel-sol transition of flow-aligned filaments measured in bulk solu-

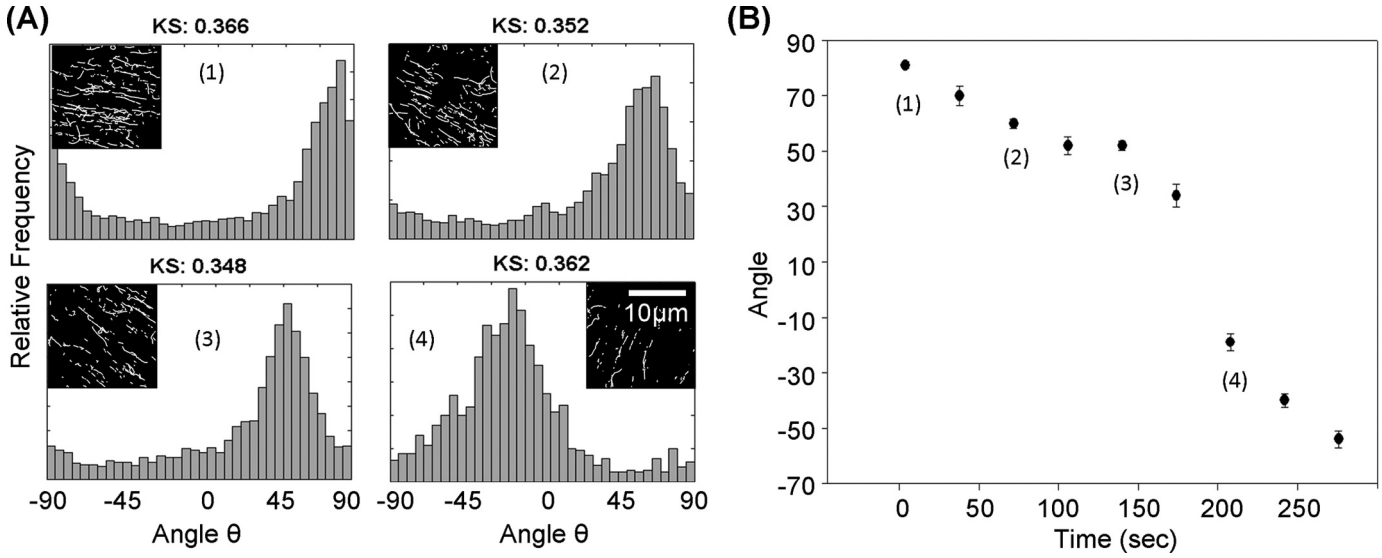

FIGURE 9. **Rotational re-alignment of an oriented domain of sliding actin filaments.** *A*, histograms of the angular distribution of trajectories and images of the filament tracks (*inset*) show how the preferred angle, θ, varies with time. Although the filament sliding speed remained approximately constant (2.7 $\pm$ 0.05 μm/s) during the experiment the preferred angle of sliding changed dramatically. *B*, the graph shows the modal value of θ plotted against time. Each value was determined from a 4-s sequence of video data and each recording was separated by a period of 30 s. The example data shown in *A* are identified by corresponding *numbers* marked on the graph.

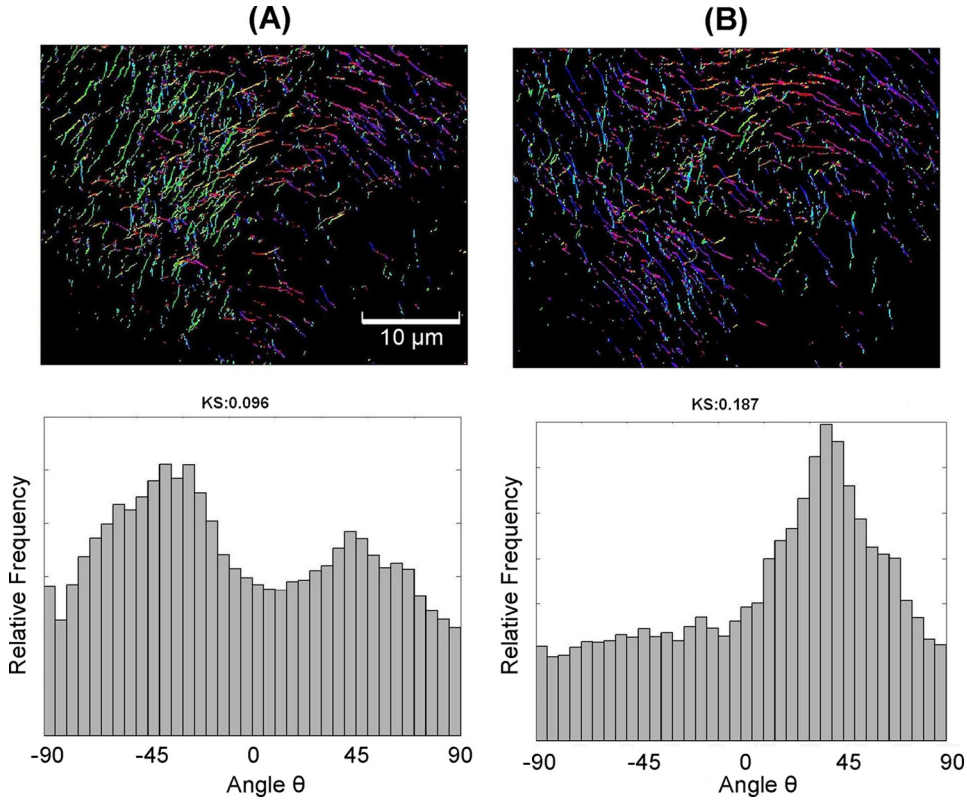

FIGURE 10. **Distinct spatial domains of aligned actin filament sliding and their temporal variation.** *A*, track record (*upper panel*) and θ distribution (*lower panel*) of a video field in which two juxtaposed domains are seen. In one region, the actin filaments move with a preferred angle of about $-45°$ relative to the horizontal and in the other at about $+45°$. *B*, track record (*upper*) and angular distribution (*lower*) of the same video field 6 s later. The field is now occupied by a single domain, moving at a preferred angle of $+45°$.

tion (20). We found alignment depended upon filament length, filament surface density, and required the action of myosin molecular motors to drive the process. The surface alignment that we observe differs from solution flow-induced alignment in the following ways. 1) It is self-induced. 2) It is generated by actomyosin motility rather than thermal motion or bulk flow. 3) The aligned patterns extend over distances of only 100 μm and/or the direction of alignment is highly variable, so would average zero in a bulk measurement.

We propose that the observed phenomena may mimic the dynamics of actin filaments at the rear region of the lamellipodium of migrating cells. The orientation of myosin molecules in our *in vitro* assays is random and yet the motion of actin was highly oriented and the preferred direction of travel could readily rotate with respect to the surface over a period of a minute. Myosin motors situated in the lamellipodium also probably have random orientation with respect to the axis of the cell yet they might produce highly directed bulk movement of actin due to lateral mechanical interactions between filaments. The density of myosin II in different cells varies widely: muscle myosin is present at 100 mg/ml in muscle cells, whereas non-muscle myosin IIa and IIb is present at about 0.2 mg/ml in platelets.[6] We applied between 0.2 and 0.5 mg/ml of myosin (HMM or thick filaments), which gives an average density of myosin heads similar

[6] J. R. Sellers, personal communication.

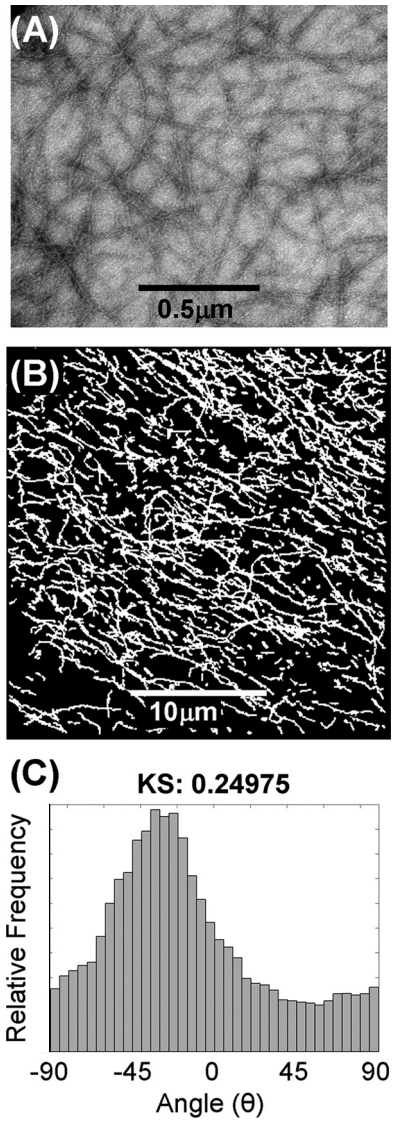

FIGURE 11. *A*, negatively stained myosin thick filaments visualized by transmission electron microscopy. *B*, myosin filaments were deposited at similar density to those shown in *A* on the *in vitro* motility assay surface and highly oriented actin gliding motility was observed in the presence of 2 mg/ml added unlabeled F-actin. *C*, analysis of the gliding orientation of the individual actin filaments shows that motion is strongly oriented (KS = 0.25), similar to findings with heavy meromyosin (compare with Fig. 2, *C* and *D*). *KS*, Kuiper statistic.

to that on a thick filament. So our assay conditions are not that dissimilar to the lamellipodium of a migrating cell in terms of the oligomeric state and concentration of myosin. Our observation that adjacent domains moving with different orientations interact and yield new patterns of motion over a period of a few seconds (*e.g.* Fig. 10) might be highly analogous to the mechanism underlying changes in direction of cell migration.

Lamellipodia are packed with actin filaments and during cell migration the lamellipodial extension rapidly explores many orientations to identify the optimal one. In simplified cell motility assay systems (11) it was discovered that application of small external forces applied using a micropipette were sufficient to guide the direction of translocating cytoplasts. This macroscopic phenomenon might be explained by the mechanism that we report here; applied external forces would perturb or add to the lateral forces between filaments that would then cause them to realign. A possible future avenue for study would be to try and forcibly align filaments within our assay either by local flow or local activation or inactivation of the myosin motors. Our present results imply that much of the dynamic behavior of lamellipodia might be controlled by alignment of sliding actin filaments in the myosin-rich region of the lamellipodium, located toward the rear region of the cell. This region has been proposed to be the "driving seat" where signals controlling cell migration are integrated (16). Cooperative, lateral mechanical interactions between actin filaments in this region of the cell might steer or bias the direction of lamellipodial protrusions further forward. Both the length and time scales of our observations seem completely consistent with this idea. Much is known about the dynamic nature of the actin meshwork at the leading edge of the cell (10, 13) and the current consensus is that actin polymerization in this region is the major force generator. Our proposal is that the direction of protrusion is steered by alignment of actin at the rear of the cell and that this process results from lateral mechanical interactions between filaments driven by myosin motors.

Finally, it is noteworthy that the myosins (8, 30) thought to be involved in lamellipodial extrusion probably have a duty cycle ratio somewhere between that typical of processive motors like myosin V and the low duty ratio motors like muscle myosin II (31, 32). This means that actin filaments would be periodically released from the myosin during the ATPase cycle so that they could move laterally to explore new directions of travel in response to lateral forces exerted by near neighbor filaments.

REFERENCES

1. Yanagida, T., Nakase, M., Nishiyama, K., and Oosawa, F. (1984) *Nature* **307,** 58–60
2. Kron, S. J., and Spudich, J. A. (1986) *Proc. Natl. Acad. Sci. U.S.A.* **83,** 6272–6276
3. Mizuno, D., Tardin, C., Schmidt, C. F., and Mackintosh, F. C. (2007) *Science* **315,** 370–373
4. Bunk, R., Klinth, J., Montelius, L., Nicholls, I. A., Omling, P., Tågerud, S., and Månsson, A. (2003) *Biochem. Biophys. Res. Commun.* **301,** 783–788
5. Howard, J. (1997) *Nature* **389,** 561–567
6. Bresnick, A. R. (1999) *Curr. Opin. Cell Biol.* **11,** 26–33
7. Diefenbach, T. J., Latham, V. M., Yimlamai, D., Liu, C. A., Herman, I. M., and Jay, D. G. (2002) *J. Cell Biol.* **158,** 1207–1217
8. Wylie, S. R., and Chantler, P. D. (2001) *Nat. Cell Biol.* **3,** 88–92
9. Small, J. V., Stradal, T., Vignal, E., and Rottner, K. (2002) *Trends Cell Biol.* **12,** 112–120
10. Pollard, T. D. (2003) *Nature* **422,** 741–745
11. Verkhovsky, A. B., Svitkina, T. M., and Borisy, G. G. (1999) *Curr. Biol.* **9,** 11–20
12. Theriot, J. A., and Mitchison, T. J. (1991) *Nature* **352,** 126–131
13. Pollard, T. D., and Borisy, G. G. (2003) *Cell* **112,** 453–465
14. Takenawa, T., and Miki, H. (2001) *J. Cell Sci.* **114,** 1801–1809
15. Symons, M. H., and Mitchison, T. J. (1991) *J. Cell Biol.* **114,** 503–513
16. Ridley, A. J., Schwartz, M. A., Burridge, K., Firtel, R. A., Ginsberg, M. H., Borisy, G., Parsons, J. T., and Horwitz, A. R. (2003) *Science* **302,** 1704–1709
17. Hall, A. (1994) *Annu. Rev. Cell Biol.* **10,** 31–54
18. Wagner, B., Tharmann, R., Haase, I., Fischer, M., and Bausch, A. R. (2006) *Proc. Natl. Acad. Sci. U.S.A.* **103,** 13974–13978
19. Wiggins, C. H., Riveline, D., Ott, A., and Goldstein, R. E. (1998) *Biophys. J.* **74,** 1043–1060
20. Janmey, P. A., Hvidt, S., Käs, J., Lerche, D., Maggs, A., Sackmann, E.,

Schliwa, M., and Stossel, T. P. (1994) *J. Biol. Chem.* **269,** 32503–32513
21. Sheetz, M. P., Block, S. M., and Spudich, J. A. (1986) *Methods Enzymol.* **134,** 531–544
22. Work, S. S., and Warshaw, D. M. (1992) *Anal. Biochem.* **202,** 275–285
23. Marston, S. B., Fraser, I. D., Bing, W., and Roper, G. (1996) *J. Muscle Res. Cell Motil.* **17,** 497–506
24. Uttenweiler, D., Veigel, C., Steubing, R., Götz, C., Mann, S., Haussecker, H., Jähne, B., and Fink, R. H. (2000) *Biophys. J.* **78,** 2709–2715
25. Mashanov, G. I., and Molloy, J. E. (2007) *Biophys. J.* **92,** 2199–2211
26. Margossian, S. S., and Lowey, S. (1982) *Methods Enzymol.* **85,** 55–71
27. Pardee, J. D., and Spudich, J. A. (1982) *Methods Enzymol.* **85,** 164–181
28. Isambert, H., Venier, P., Maggs, A. C., Fattoum, A., Kassab, R., Pantaloni, D., and Carlier, M. F. (1995) *J. Biol. Chem.* **270,** 11437–11444
29. Kuiper, N. H. (1962) *Proc. Kon. Ned. Akad. Wetensc.* **63,** 38–47
30. Verkhovsky, A. B., Svitkina, T. M., and Borisy, G. G. (1995) *J. Cell Biol.* **131,** 989–1002
31. Wang, F., Kovacs, M., Hu, A., Limouze, J., Harvey, E. V., and Sellers, J. R. (2003) *J. Biol. Chem.* **278,** 27439–27448
32. Kovács, M., Wang, F., Hu, A., Zhang, Y., and Sellers, J. R. (2003) *J. Biol. Chem.* **278,** 38132–38140